HHS Public Access

Author manuscript

Cell Metab. Author manuscript; available in PMC 2020 April 02.

Published in final edited form as:

Cell Metab. 2019 April 02; 29(4): 966–978.e4. doi:10.1016/j.cmet.2019.01.016.

Glutamine metabolism regulates proliferation and lineage allocation in skeletal stem cells

Yilin Yu[1], **Hunter Newman**[1], **Leyao Shen**[1], **Deepika Sharma**[1], **Guoli Hu**[1], **Anthony J. Mirando**[1], **Hongyuan Zhang**[1], **Everett Knudsen**[1], **Guo-Fang Zhang**[2,3], **Matthew J. Hilton**[1,4], **Courtney M. Karner**[1,4,5,*]

[1]Department of Orthopaedic Surgery, Duke Orthopaedic Cellular, Developmental and Genome Laboratories, Duke University School of Medicine, Durham, NC 27710, USA

[2]Sarah W. Stedman Nutrition and Metabolism Center & Duke Molecular Physiology Institute, Duke University Medical Center, 300 North Duke Street, Durham, NC 27701, USA

[3]Department of Medicine, Duke University School of Medicine, Durham NC 27701, USA

[4]Department of Cell Biology, Duke University, Durham, NC 27710, USA

[5]Lead Contact.

Summary:

Skeletal stem cells (SSC) are postulated to provide a continuous supply of osteoblasts throughout life. However, under certain conditions, the SSC population can become incorrectly specified or is not maintained, resulting in reduced osteoblast formation, decreased bone mass, and in severe cases osteoporosis. Glutamine metabolism has emerged as a critical regulator of many cellular processes in diverse pathologies. The enzyme glutaminase (GLS) deaminates glutamine to form glutamate, the rate-limiting first step in glutamine metabolism. Using genetic and metabolic approaches, we demonstrate GLS and glutamine metabolism is required in SSC to regulate osteoblast and adipocyte specification and bone formation. Mechanistically, transaminase dependent α-ketoglutarate production is critical for the proliferation, specification and differentiation of SSC. Collectively, these data suggest stimulating GLS activity may provide a therapeutic approach to expand SSCs in aged individuals and enhance osteoblast differentiation and activity to increase bone mass.

Keywords

glutamine metabolism; glutaminase; skeletal stem cell; lineage specification; osteoporosis

*Correspondence: Courtney.Karner@duke.edu.

Author Contributions

Conceptualization, C.M.K; Investigation, Y.Y., H.N., L.S., D.S., G.H., A.J.M., H.Z., E.K., G.Z., M.J.H, and C.M.K.; Writing – Original Draft, C.M.K; Writing – Review & Editing, G.Z., M.J.H. and C.M.K.; Supervision, C.M.K.

Declaration of Interests

The authors declare no competing interests.

Introduction:

Osteoporosis is a prevalent human disease characterized by low bone mass and deterioration of the bone microarchitecture resulting in increased fracture susceptibility (Eisman, et al., 2012; 2004). Osteoporosis affects approximately 10 million Americans over the age of 50 and is estimated to cost upwards of 20 billion dollars per annum (Becker, et al., 2010). Adult bone is a dynamic tissue undergoing constant remodeling, which is regulated by both the number and cellular activity of the bone forming osteoblasts and bone resorbing osteoclasts. Skeletal stem cells (SSC), also termed bone marrow mesenchymal stromal cells (BMSC) are critical regulators of postnatal bone homeostasis by providing a reservoir of osteoblasts throughout life (Bianco and Robey, 2015; Mizoguchi, et al., 2014; Zhou, et al., 2014). Originally, SSC were defined by multiple characteristics including adherence to plastic, ability to generate fibroblastic colonies (CFU-F) in culture and the capability to differentiate into adipocytes, osteoblasts and chondrocytes *in vitro* (Bianco and Robey, 2015; Owen and Friedenstein, 1988; Friedenstein, et al., 1966). Recent studies have demonstrated SSC arise postnatally, are tightly associated with the vasculature *in vivo* and can be targeted in mouse using various Cre lines including *Prx1Cre* and *LeprCre* (Mizoguchi, et al., 2014; Zhou, et al., 2014; Ding and Morrison, 2013; Greenbaum, et al., 2013). Under normal physiological conditions, SSC are quiescent, but rapidly proliferate and can differentiate into adipocytes, osteoblasts and chondrocytes in response to injury (Zhou, et al., 2014; Park, et al., 2012). With age, SSC numbers decline. This results in decreased osteoblast generation, leading to decreased bone mass and diminished regeneration potential over time. Moreover, the differentiation potential of SSC shifts to favor adipogenesis with age further decreasing osteoblast generation and bone formation (Moerman, et al., 2004; Justesen, et al., 2001; D'Ippolito, et al., 1999; Nishida, et al., 1999). Recent studies have identified many extrinsic signals that regulate SSC lineage commitment and differentiation (Fairfield, et al., 2018; Balani, et al., 2017; Fan, et al., 2017; Wu, et al., 2017; Yue, et al., 2016; Li, et al., 2013). However, the intrinsic mechanisms governing SSC commitment to the osteogenic rather than adipogenic lineage remain to be elucidated.

Glutamine metabolism is emerging as an intriguing regulatory node frequently altered in many pathological conditions (Still and Yuneva, 2017; Zhang, et al., 2017; Karner, et al., 2015). Glutamine is the most abundant nonessential amino acid in circulation and has multiple metabolic uses in the cell (Stein and Moore, 1954). Glutamine metabolism is initiated by the enzyme glutaminase (GLS), which deaminates it to form glutamate, an important intermediate metabolite which has many biosynthetic uses in the cell. The physiological role of glutamine metabolism during embryonic and postnatal development is unknown as mice deficient for *Gls* die within 24 hours of birth due to defects in glutamatergic neural transmission (Masson, et al., 2006). However, no other phenotypes were reported in these mice suggesting glutamine metabolism is not important physiologically. On the contrary, much is known about the importance of glutamine metabolism in pathological conditions. For example, some tumor cells utilize glutamine metabolism to provide NADPH and better utilize glucose carbons to generate biomass (DeBerardinis, et al., 2007). In other tumors, glutamine metabolism provides carbon for lipid and glutathione biosynthesis as well as nitrogen for nucleotide biosynthesis to control

oxidative stress and support proliferation (Le, et al., 2012; Metallo, et al., 2011; Mullen, et al., 2011; Wise, et al., 2011; Wise and Thompson, 2010; DeBerardinis, et al., 2007). It is unknown if SSC utilize glutamine metabolism and if so what it is used for.

Here we define the role of glutamine metabolism during physiological bone formation and homeostasis. We describe the distinct requirement for glutamine metabolism in SSC to maintain bone homeostasis. Using genetic and metabolic approaches, we demonstrate GLS activity and glutamine metabolism regulates SSC proliferation and appropriate lineage allocation in mice. Collectively, our data highlight the previously unknown role for glutamine metabolism in SSC regulating physiological bone formation.

Results:

Differential requirements for glutamine metabolism during mesenchymal stem cell differentiation.

Upon examination of the metabolic needs of skeletal stem cells (SSC) in culture we observed a significant increase in glutamine consumption during osteoblast differentiation (Figure 1A, C and Figure S1A). Likewise, GLS activity was markedly increased during osteoblast differentiation (Figure 1D). Conversely, during adipocyte differentiation, neither glutamine consumption nor GLS activity were altered relative to undifferentiated SSC (Figure 1B–D and Figure S1B). To determine if exogenous glutamine is required for SSC differentiation, we cultured SSC under osteogenic or adipogenic conditions in the presence or absence of glutamine supplementation. SSC underwent robust differentiation into either osteoblast or adipocyte lineages when cultured in the presence of exogenous glutamine (Figure 1E–F, Figure S1C–D). Glutamine withdrawal reduced SSC differentiation into the osteoblast lineage as exemplified by reduced matrix mineralization and decreased marker gene expression (Figure 1E and Figure S1C). Conversely, glutamine withdrawal increased adipocyte marker gene expression and lipid accumulation during adipocyte differentiation (Figure 1F and Figure S1D). These data suggest SSC utilize glutamine disparately during differentiation into osteoblast and adipocyte lineages.

GLS is the primary enzyme responsible for glutamine catabolism. GLS activity is encoded by two protein isoforms, Kidney type Glutaminase A (KGA, encoded by *Gls*) and Liver type Glutaminase (LGA, encoded by *Gls2*). Quantitative PCR (qPCR) analyses demonstrated that SSC express *Gls* at much higher levels than *Gls2* in both the undifferentiated and differentiated conditions (Figure 1G and S1E). Moreover, *Gls2* expression was negligible, suggesting *Gls* encodes the majority of GLS activity in SSC. To test this hypothesis, we inhibited KGA using the small molecule inhibitor Bis-2-(5-phenylacetamido-1,3,4-thiadiazol-2-yl)ethyl sulfide (BPTES) (Thangavelu, et al., 2012). BPTES treatment significantly reduced ^{3}H-glutamate production from L-[2,3,4-^{3}H] glutamine confirming *Gls* encodes the primary GLS isoform expressed in SSC (Figure 1H).

We next sought to understand how glutamine is utilized during osteoblast differentiation. First, we determined the effect of GLS inhibition on downstream metabolites using mass spectrometry. GLS inhibition significantly diminished intracellular glutamate and α-ketoglutarate (αKG) as well as the downstream products aspartate and alanine (Figure 1I).

Conversely, GLS inhibition had no effect on other products of glutamine metabolism (e.g. proline) (Figure 1I). Next, we used stable isotopically labeled glutamine to trace the relative metabolic fluxes of glutamine. Briefly, SSC precultured in growth or osteogenic media for 7 days were incubated with a glutamine tracer uniformly labeled with ^{13}C ([U-^{13}C]glutamine) for 1 hour, and contribution of the tracer to downstream metabolites was determined by measuring the mass isotope-labeling pattern (Figure 1J). As a control, SSC were cultured in BPTES for 1 hour prior to the 1 hour incubation with [U-^{13}C]glutamine. As expected, a significant amount of glutamate was derived from glutamine (Figure 1K and Figure S1F). Likewise, glutamine carbon contributed to the TCA cycle (e.g. citrate) and was used for amino acid (e.g. proline, aspartate and alanine) and glutathione biosynthesis (Figure S1G–J). Importantly, glutamine contribution to citrate, amino acid and glutathione biosynthesis was prevented by BPTES treatment (Figure S1F–J). We next evaluated glutamine metabolism in SSC during osteoblast differentiation. Glutamine contributed to citrate both through oxidation (M+4) and reductive carboxylation (M+5) in undifferentiated SSC (Figure 1L). Glutamine contribution to citrate (both M+4, and M+5) was significantly reduced in differentiated SSC (Figure 1L). This is likely the result of higher glucose flux associated with osteoblast differentiation which dilutes the labeling from glutamine. Conversely, glutamine contribution to aspartate and other amino acids remained consistent during differentiation (Figure 1M and Figure S1M). These data suggest that in differentiated SSC glutamine carbon is used primarily to provide α-ketoglutarate which contributes to amino acid biosynthesis in SSC.

Gls is required for bone formation *in vivo*

To determine the role of *Gls* during bone formation directly, we deleted a conditionally null (floxed) allele of *Gls* (*Gls*^{fl}) in the mesenchymal progenitor cells of the limb bud using the *Prx1Cre* deleter mouse (Masson, et al., 2006; Logan, et al., 2002). *Prx1Cre* is expressed throughout the limb bud mesenchyme beginning at embryonic day 9.5 and is expressed in chondrocytes and during all stages of osteoblast differentiation (Figure S2A,E). *Prx1Cre;Gls*$^{fl/fl}$ mice were born at Mendelian ratios and were indistinguishable from wild type littermates at birth despite loss of GLS protein expression (Figure S2B–D). X-ray analyses of 4-month old mice demonstrate the long bones from *Prx1Cre;Gls*$^{fl/fl}$ mice are overtly normal with no defects in length, growth or morphology relative to wild type littermates (Figure S2F). These analyses did identify a reduction in overall bone mass in *Prx1Cre;Gls*$^{fl/fl}$ mice relative to wild type littermates (Figure S2F). μCT analyses confirmed that *Gls* deletion resulted in a significant reduction in bone mass (Figure 2A–B). Quantification of the μCT analyses demonstrated that *Gls* deletion resulted in significant reductions in trabecular bone volume per tissue volume (BV/TV), trabecular number (Tb.N) and bone mineral density (BMD), while increasing trabecular separation (Tb.Sp) in both males and females at 4 months of age (Figure 2A–B, Table S1). *Gls* deletion also affected cortical bone highlighted by decreased cortical thickness (Ct.Th) with no change in total bone area (T.Ar) (Figure 2C–D, Table S1). Histological analyses confirmed a significant reduction in trabecular bone underneath the growth plate (Figure 2E–F). These analyses highlighted a partially penetrant sex dependent increase in marrow adiposity evident in 75% of *Prx1Cre;Gls*$^{fl/fl}$ female mice compared to wild type littermates at this time point (Figure 2E–F, p=0.0022, binomial test). OsO_4 enhanced μCT analyses confirmed the presence of

increased adiposity in the distal femurs of *Prx1Cre;Gls*$^{fl/fl}$ female mice (Figure 2G and S2G). Because adipocytes and osteoblasts share a common progenitor we next evaluated if *Gls* ablation affected osteoblast endowment using static histomorphometry (Figure 2H–I). Quantification of the histomorphometric data identified a significant reduction in the overall number of osteoblasts per bone surface (Ob.N/BS) in both males and females (Figure 2H–I). Similarly, we observed a significant reduction in osteoblast specific gene and protein expression in bone extracts from *Prx1Cre;Gls*$^{fl/fl}$ mice (Figure S2H–I). Similarly, we observed a significant reduction in osteoblast specific gene and protein expression in bone extracts from *Prx1Cre;Gls*$^{fl/fl}$ mice (Figure S2H–I). Importantly, *Gls* deletion did not affect bone resorption as we observed no change in TRAP stained osteoclasts per bone surface (Figure 2J–K). We next used dynamic histomorphometry to evaluate bone formation directly (Figure 2L–O). *Prx1Cre;Gls*$^{fl/fl}$ mice have a significant reduction in osteoblast coverage as exemplified by the mineralized surface per bone surface (MS/BS) (Figure 2M). Not only were there fewer osteoblasts in *Prx1Cre;Gls*$^{fl/fl}$ mice, but they displayed less bone forming activity as both the mineral apposition rate (Korangath, et al.) and bone formation rate (BFR) were significantly decreased in *Prx1Cre;Gls*$^{fl/fl}$ mice relative to littermate controls (Figure 2N–O). Thus, *Gls* dependent glutamine metabolism is required for normal mesenchymal lineage allocation, osteoblast endowment and bone mass accrual *in vivo*.

Glutamine metabolism is required for appropriate specification of SSC

We next determined how *Gls* deletion affected osteoblast endowment. We first evaluated if *Gls* deletion affected SSC maintenance and specification by performing colony forming efficiency (CFE) assays in 2-month-old *Prx1Cre;Gls*$^{fl/+}$ (Wild Type) and *Prx1Cre;Gls*$^{fl/fl}$ mice. *Prx1Cre;Gls*$^{fl/fl}$ mice displayed normal CFE indicating the SSC population of the bone marrow was normal (Figure 3A–C). We next stained colonies for alkaline phosphatase expression (CFU-AP) to evaluate osteoblastic specification of SSC. *Gls* deletion resulted in reduced osteoblast specification of SSC as we observed a significant reduction in alkaline phosphatase positive colonies relative to overall CFE (Figure 3D–F). To test if the change in specification was functional we treated colonies from wild type and *Prx1Cre;Gls*$^{fl/fl}$ mice with either osteogenic or adipogenic media for an additional fourteen days and evaluated differentiation potential. There was a significant reduction in the numbers of Von Kossa stained osteoblastic colonies (CFU-Ob) from *Prx1Cre;Gls*$^{fl/fl}$ mice (Figure 3G–I). Conversely, colonies isolated from *Prx1Cre;Gls*$^{fl/fl}$ mice demonstrated a significant increase in adipogenic potential as shown by increased Oil Red-O staining (CFU-Ad) (Figure 3J–L). These data indicate that *Gls* and glutamine metabolism is required for normal SSC specification and appropriate lineage allocation. To test if *Gls* ablation affects differentiation ability directly we performed high density SSC cultures isolated from either wild type or *Prx1Cre;Gls*$^{fl/fl}$ littermates. SSC isolated from *Prx1Cre;Gls*$^{fl/fl}$ mice were able to undergo osteoblast differentiation but displayed diminished matrix mineralization as well as reduced osteoblast marker gene expression (Figure S3A–B). GLS knockout did not affect viability in SSC as we observed no increase in cleaved Caspase 3 suggesting the reduction in osteoblast marker gene expression and mineralization is the result of reduced osteoblast differentiation (Figure S3C). Conversely, *Prx1Cre;Gls*$^{fl/fl}$ SSC underwent normal adipogenic differentiation shown by Oil Red O staining and marker gene expression (Figure S3D–E). Unexpectedly, when cultured in media containing both adipogenic and osteogenic cues, *Prx1Cre;Gls*$^{fl/fl}$

SSC displayed enhanced adipocyte differentiation *in vitro,* with increased Oil Red O staining and adipogenic gene expression (Figure 3M–N). Conversely, wild type SSC preferentially differentiated into osteoblasts (Figure 3M–N). Thus, *Gls* and glutamine metabolism are critical for lineage specification and differentiation of bone marrow SSC.

Collectively, our data indicates *Gls* and glutamine metabolism regulates osteoblast specification, differentiation and bone formation. Because *Prx1Cre;Gls*$^{fl/fl}$ mice lack a bone phenotype prior to 2 months of age despite deletion of *Gls* in all osteoblast lineage cells, we hypothesized *Gls* is required directly in the SSC. Consistent with this hypothesis, deletion of *Gls* in mature osteoblasts using *BglapCre* had no effect on either bone mass or osteoblast or osteoclast numbers at 4 months of age suggesting *Gls* is dispensable in mature osteoblasts (Figure S4 and Table S2). To test the role of *Gls* in SSC directly we deleted *Gls* using the *LeprCre* deleter strain that is active in SSC that give rise to osteoblasts postnatally (Figure S5) (Mizoguchi, et al., 2014; Zhou, et al., 2014). μCT analyses demonstrated that while *LeprCre;Gls*$^{fl/fl}$ mice had no bone phenotype at 2 months, they had a significant decrease in bone mass in both males and females at 4 months (Figure 4A–B, Table S3 and data not shown). The decreased bone mass in *LeprCre;Gls*$^{fl/fl}$ mice was mainly attributed to decreased trabecular numbers and increased trabecular separation (Table S3). Decreased bone mass was not the result of increased bone resorption as we found no change in the number of TRAP positive osteoclasts in *LeprCre;Gls*$^{fl/fl}$ mice (Figure 4C–E). Conversely, *LeprCre;Gls*$^{fl/fl}$ mice had significantly fewer Osteocalcin (OCN) positive osteoblasts compared to wild type littermates (Figure 4H–J). Dynamic histomorphometry revealed a significant decrease in MS/BS, MAR and BFR specifically in the trabecular and endosteal but not periosteal compartments of *LeprCre;Gls*$^{fl/fl}$ mice (Table S3). Importantly, we did not observe increased apoptosis in LeprCre expressing cells or their derivatives (Figure S5E).

The bone phenotype of *LeprCre;Gls*$^{fl/fl}$ mice was reminiscent of the *Prx1Cre;Gls*$^{fl/fl}$ phenotype. We next sought to determine if there was a similar marrow adiposity phenotype in these mice. Histological analyses highlighted a partially penetrant sex dependent increase in marrow adiposity evident in 67% of *LeprCre;Gls*$^{fl/fl}$ female compared to littermate controls at 4 months of age (n=7, $p \leq 0.00001$, binomial test) (Figure S5C). OsO_4 enhanced μCT analysis confirmed the presence of increased marrow fat in tibiae isolated from *LeprCre;Gls*$^{fl/fl}$ female mice (Figure 4F–G and S5D). Immunofluorescent staining for the adipocyte marker Perilipin (PLIN) confirmed the presence of adipocytes in the bone marrow of *LeprCre;Gls*$^{fl/fl}$ female mice (Figure 4K–L). Importantly, in both wild type and *LeprCre;Gls*$^{fl/fl}$ mice, almost all PLIN^{+} adipocytes also expressed tdTomato (88.1±16.9% vs 97.8±2.6%, wild type vs *LeprCre;Gls*$^{fl/fl}$ respectively) indicating they were derived from *LeprCre* expressing SSC (Figure 4K–L). These data suggest *Gls* and glutamine metabolism are required cell autonomously for appropriate lineage allocation and osteoblast differentiation in SSC.

Gls is required for SSC proliferation

We next evaluated the CFE of *LeprCre;Gls*$^{fl/fl}$ mice. Surprisingly, *LeprCre;Gls*$^{fl/fl}$ mice displayed a significant reduction in CFE (Figure 5A–B). It is important to note that although the overall number of colonies containing at least 50 cells was significantly reduced in

LeprCre;Gls$^{fl/fl}$ mice, there was no difference in the number of colonies containing at least 10 cells (Figure 5C). Indeed, there was a significant bias toward smaller colonies with fewer cells in *LeprCre;Gls*$^{fl/fl}$ mice (Figure 5D, $p<0.0005$, binomial test, $n\geq213$ colonies for each genotype). To determine if *Gls* and glutamine metabolism in SSC regulates overall SSC numbers or proliferation we performed CFE assays on cells isolated from *C57Bl/6* mice in media containing either 2 or 0mM glutamine. Importantly, either glutamine withdrawal or GLS inhibition significantly reduced the number of colonies containing at least 50 cells and decreased the number of cells per colony (Figure 5E–H and Figure S6A–B). These data indicate that *Gls* ablation does not affect overall SSC numbers in the bone marrow but may govern SSC proliferation. To test this hypothesis, we cultured SSC isolated from *C57Bl/6* mice in the presence or absence of exogenous glutamine and evaluated proliferation. SSC cultured without exogenous glutamine displayed a significant reduction in EDU incorporation (Figure 5I). Similarly, GLS inhibition significantly reduced both overall cell numbers and EDU incorporation in SSC (Figure 5J and Figure S5C–E). Western blot analyses demonstrate that inhibiting GLS activity significantly reduces both Cyclin D1 and D3 expression (Figure 5K–L) indicating GLS activity is required for SSC proliferation. In support of this, we observed decreased BrdU incorporation in both Prx1Cre;Gls$^{fl/fl}$ and LeprCre;Gls$^{fl/fl}$ mice relative to wild type controls (Figure S6F). Taken together, our data indicate GLS activity and glutamine metabolism are required for appropriate SSC proliferation.

Our metabolic analyses indicated that αKG is a primary product of glutamine metabolism in SSC (Figure 1I). To test if glutamine derived αKG is important for colony expansion we performed rescue experiments. αKG supplementation, but not other metabolites (e.g. nucleotides or GSH), rescued colony expansion in the absence of exogenous glutamine (Figure 6A–B). We next sought to understand how SSC generate αKG from glutamine. The amino acid transaminases utilize the α nitrogen from glutamate for the biosynthesis of amino acids like aspartate and alanine whereas glutamate dehydrogenase deaminates glutamate to form ammonia. To determine if the transaminases are active in SSC we incubated SSC with a glutamine tracer labeled with ^{15}N on the α nitrogen ($^{15}N_{\alpha}$-glutamine) for 1 hour, and the contribution of the tracer to glutamate, aspartate and alanine was determined by measuring the mass isotopologue-labeling pattern (Figure 6C). The glutamine α nitrogen is highly enriched in glutamate (M+1) as well as in both aspartate (M+1) and alanine (M+1) suggesting SSC have high amino acid transaminase activity (Figure 6D). Importantly, GLS inhibition prevented glutamine derived nitrogen contribution to glutamate, aspartate or alanine (Figure 6D). Functionally, inhibiting amino acid transaminase activity using the drug AOA significantly reduced colony formation similar to GLS inhibition (Figure 6E–F) (Korangath, et al., 2015; Kauppinen, et al., 1987). Conversely, glutamate dehydrogenase inhibition using Bithionol had no effect on colony formation (Figure 6E–F) (Li, et al., 2009). Collectively these data indicate that amino acid transaminase dependent αKG production is critical for SSC proliferation and colony expansion.

Discussion

We show here that glutamine metabolism is a critical regulator of SSC proliferation, lineage allocation and osteoblast differentiation. SSC consume and metabolize a significant amount

of glutamine as they undergo differentiation into the osteoblast but not adipocyte lineage. Genetically inhibiting glutamine metabolism in SSC results in decreasing bone mass with age, a hallmark of age-associated osteoporosis. Mechanistically, decreased bone mass is the result of multiple factors: first, a reduction in overall osteoblast numbers. This is likely the result of decreased proliferation and altered lineage allocation favoring the adipocyte lineage in *Gls* deficient SSC. Second, GLS deficient osteoblasts have reduced bone formation. Collectively these data provide the first example of the critical role of glutamine metabolism in SSC to regulate lineage allocation and bone homeostasis in mice.

SSC give rise to both osteoblasts and adipocytes throughout life. Interestingly, bone mass and marrow adiposity are known to be negatively correlated. The loss of *Gls* in SSC resulted in decreased bone mass in both males and females and increased marrow adiposity apparent only in female mice. It is unclear from these experiments if males have a similar adiposity phenotype as we only evaluated mice at 4 months of age, thus it is possible male mice at older time points also have increased adiposity. However, marrow adiposity, much like bone mass is a sexually dimorphic trait. Female mice have lower bone mass and are reported to have over 10 times more marrow adipocytes in the proximal tibia relative to male mice (Lecka-Czernik, et al., 2017). Thus, it is plausible that extrinsic factors disparately influence marrow adiposity in male and female mice. Importantly, SSC from male *Gls* knockout mice were more receptive to adipogenic cues *in vitro* supporting an intrinsic role for glutamine metabolism in lineage specification (Figure 3). Future studies are needed to understand this phenomenon.

SSC metabolize glutamine to support both proliferation and osteoblast specification. Glutamine has long been recognized as an important nutrient in proliferating cells in culture (Eagle, et al., 1956; Eagle, 1955). Glutamine is essential to progress through both the G1 restriction point as well as exit S phase to begin cell division (Colombo, et al., 2011). Consistent with these data, inhibition of GLS in SSC reduced the expression of cell markers Cyclin D1 and D3 as well as EDU incorporation (Figure 5I–L). This is consistent with a recent report demonstrating glutamine metabolism is required to support endothelial cell proliferation *in vivo* (Huang, et al., 2017; Kim, et al., 2017). Our data demonstrate that amino acid transaminase derived αKG is the critical downstream metabolite regulating proliferation in SSC (Figure 1I and Figure 6). Aspartate biosynthesis was reported to be critical for proliferation by providing carbon and nitrogen for synthetic reactions necessary for proliferation (Birsoy, et al., 2015; Sullivan, et al., 2015). Future studies are warranted to determine if glutamine dependent aspartate biosynthesis contributes to proliferation in SSC.

During our CFU analyses comparing the *Prx1Cre;Gls*$^{fl/fl}$ and *LeprCre;Gls*$^{fl/fl}$ mice we uncovered an apparent disparity in the CFE between mutant genotypes. One would predict that the CFE would be similar between these mutant genotypes, however *LeprCre;Gls*$^{fl/fl}$ mutants exhibit fewer CFU-F while *Prx1Cre;Gls*$^{fl/fl}$ mutants show no significant difference compared to controls. There are two possible explanations for this. First, based on the expression of both *Prx1Cre* and *LeprCre* (Figures S2 and S4), *Gls* deletion using *LeprCre* might place *Gls* null SSC at a competitive disadvantage relative to surrounding wild type cells able to utilize glutamine to support proliferation (Zhou, et al., 2014; Logan, et al., 2002). By comparison, *Prx1Cre* is more broadly expressed in the bone marrow resulting in

less of a competitive disadvantage for *Gls* null SSC and minimal effect on proliferation. Second, SSC may be addicted to glutamine metabolism to support proliferation similar to some cancer cells (Wise and Thompson, 2010). However, if SSC are derived from cells unable to metabolize glutamine they avoid the glutamine addiction and can proliferate and function normally. *Prx1Cre* is active beginning at embryonic day 9.5 in cells that give rise to the SSC population while *LeprCre* is not active until the SSC forms (Greenbaum, et al., 2013; Logan, et al., 2002). In this scenario, *Prx1Cre;Gls*$^{fl/fl}$ SSC have never been able to metabolize glutamine and have overcome this deficiency whereas *LeprCre;Gls*$^{fl/fl}$ SSC are unable to overcome the acute loss of glutamine metabolism. Our data inhibiting glutamine metabolism in otherwise wild type SSC support this hypothesis as glutamine withdrawal and GLS inhibition both phenocopied the *LeprCre;Gls*$^{fl/fl}$ CFE phenotype despite inhibiting glutamine metabolism in all plated cells (Figure 5A–G). It is important to note *Prx1Cre;Gls*$^{fl/fl}$ SSC had diminished proliferation when induced to undergo osteoblast differentiation suggesting they are unable to compensate for the loss of glutamine metabolism in certain instances (Figure 5L).

Cellular metabolism is emerging as a critical regulator of stem cell maintenance, cell fate determination and differentiation in various contexts (Oburoglu, et al., 2014; Knobloch, et al., 2013; Ito, et al., 2012). For example, alterations in glucose metabolism promotes osteoblast fate at the expense of adipocyte fate through epigenetic regulation of gene expression (Karner, et al., 2016). Similarly, our data indicates glutamine metabolism is required for appropriate lineage allocation in SSC. The precise mechanism by which glutamine metabolism acts is unknown. Lineage commitment and differentiation likely present SSC with diverse energetic, biosynthetic and antioxidant demands. For example, osteoblasts increase protein synthesis and secretion during differentiation, both energetically demanding processes. Conversely, adipocytes are known to store energy in the form of lipids. In SSC, glutamine does not appear to be a major energetic substrate as glutamine contribution to citrate declined during osteoblast differentiation and GLS inhibition did not induce energetic stress (Figure 1L and Figure S1K). We postulate glycolysis offsets this as recent reports indicate that glycolysis increases during osteoblast differentiation and that osteoblasts derive most of their ATP from glycolysis (Guntur, et al., 2014; Komarova, et al., 2000; Borle, et al., 1960). Metabolic flexibility is likely important to allow SSC to best utilize available nutrients to respond to diverse cellular demands associated with proliferation, specification and differentiation. In contrast to energetics, glutamine contribution to GSH increased during osteoblast differentiation (Figure S1K). This may be important to offset ROS known to be detrimental to the osteoblast fate (Wang, et al., 2015; Tormos, et al., 2011; Chen, et al., 2008; Almeida, et al., 2007; Bai, et al., 2004; Mody, et al., 2001). In the case of adipocyte differentiation, glutamine may be less important given the positive role of ROS (Wang, et al., 2015; Tormos, et al., 2011).

Osteoblasts are known to express an array of SIBLING (e.g. Osteopontin), GLA (e.g. Osteocalcin) and acidic glycoproteins (e.g. osteonectin and sialoprotein II) that function to regulate collagen mineralization. These proteins are significantly enriched for both aspartate and glutamate residues. Glutamine metabolism is critical to maintain levels of both glutamate and aspartate in SSC as glutamine contributes both carbon and nitrogen for glutamate and aspartate biosynthesis. It is intriguing to speculate that glutamine metabolism

fulfills this unique synthetic requirement of osteoblasts and thus promotes collagen mineralization and bone formation. Another possibility is that glutamine metabolism epigenetically regulates lineage allocation in SSC. αKG is a cofactor for both Jumonji domain containing histone demethylases and the TET family of DNA demethylases (McDonough, et al., 2010; Schofield and Zhang, 1999). A reduction in glutamine derived αKG is predicted to reduce DNA and histone demethylation potentially biasing lineage commitment. Indeed, Tet1 and Tet2 are necessary for SSC self-renewal and osteoblast differentiation (Yang, et al., 2018). Our data demonstrate GLS, and thus glutamine, is at the apex of a complex regulatory network in SSC. Future studies will be necessary to elucidate the precise mechanisms by which glutamine metabolism impacts SSC through the epigenetic regulation of osteogenic factors, the generation of amino acids critically important to specific osteoblast and bone forming proteins, and the regulation of ROS.

Limitations of the Study

In summary, while our study demonstrates the critical role of GLS and glutamine metabolism in the regulation of SSC proliferation and osteoblast endowment, the precise molecular details remain to be resolved. Our data highlight αKG as a critical regulator of SSC proliferation, however, the mechanism by which αKG regulates proliferation is unclear. Similarly, the roles of αKG during lineage allocation and osteoblast differentiation remain to be elucidated. It is important to note our data do not exclude the possibility that multiple downstream metabolites are required for osteoblast specification and differentiation in SSC. Regardless, our data highlights a previously unknown role for glutamine metabolism in regulating bone homeostasis.

STAR Methods

CONTACT FOR REAGENT AND RESOURCE SHARING

Further information and requests for reagents may be directed to and will be fulfilled by the Lead Contact, Courtney Karner (Courtney.Karner@duke.edu)

EXPERIMENTAL MODEL AND SUBJECT DETAILS

Mouse strains—*Gls*^{flox} (RRID:IMSR_JAX:017894), *Prx1Cre* (RRID:IMSR_JAX:005584), *BglapCre (*RRID:IMSR_JAX:019509), and *LeprCre* (RRID:IMSR_JAX:008320) mouse strains are as previously described (Masson, et al., 2006; Logan, et al., 2002; Zhang, et al., 2002; DeFalco, et al., 2001). *C57Bl/6J* (RRID:IMSR_JAX:000664) and *Rosa26tdTomato* (RRID:IMSR_JAX:007909) mouse strains were obtained from the Jackson Laboratory. We backcrossed all mice for 5 generations onto the C57Bl/6J background prior to experiments. Mice were housed at 23˚ C on a 12 hour light/dark cycle with free access to water and PicoLab Rodent Diet 20 (LabDiet #5053, St. Louis MO). Mice were analyzed at 4 months of age and both male and female mice were analyzed. The assessment of all animal studies were performed in a blinded and coded manner. The Animal Studies Committee at Duke University approved all mouse procedures.

Primary cells and cell lines—Primary bone marrow skeletal stem cells (SSC) were isolated from 2–4-month old male and female mice. The ST2 cell line (RRID:CVCL_2205) was obtained from RIKEN. ST2 cells were originally established from long-term bone marrow cultures of BALB/c mice, the sex of which is unknown. Cells were maintained in ascorbic acid free aMEM containing either 15% FBS for primary SSC or 10% FBS for ST2 cells. All cell culture experiments were carried out at 37˚C and 5% CO_2.

METHOD DETAILS

Mouse analyses—All mouse lines were backcrossed for 5 generations and subsequently maintained on the C57Bl/6J background prior to experiments. Radiographs of mouse skeleton were generated using a Faxitron X-ray system (Faxitron X-ray Corp) with 20-second exposure under 25 kV. Micro computed tomography (VivaCT 80, Scanco Medical AG) was used for three-dimensional reconstruction, and quantification of bone parameters (threshold set at 320) from 200 slices underneath the growth plate. For OsO_4 μCT, bones were decalcified in 14% EDTA for 2 weeks. Adipocytes were stained using OsO_4. Micro computed tomography (VivaCT 80) was used for three-dimensional reconstruction, and quantification of adiposity (threshold set at 550) from 200 slices underneath the growth plate (Scheller, et al., 2014). Bone histomorphometry was performed on femurs fixed in 10% buffered formalin overnight at 4˚C followed by 2-week decalcification in 14% EDTA. Following decalcification, bones were embedded in paraffin and sectioned at 5 μm thickness. Hematoxylin and eosin (H&E), tartrate-resistant acid phosphatase (TRAP), and Picrosirius Red/Alcian Blue (AB/PSR) staining were performed following standard protocols. For dynamic histomorphometry, mice were injected with calcein (20mg/kg) intraperitoneally at 7 and 2 days prior to sacrifice respectively. Freshly isolated bones were sucrose embedded in OCT for fresh unfixed frozen sections using cryojane. Both static and dynamic histomorphometry were quantified using ImageJ (Egan, et al., 2012). Briefly, photomicrographs were used to generate image masks representing bone and non-bone tissue. The images were used to quantify osteoblast and osteoclast numbers, bone surface, mineralizing surface, and interlabel width in Image J. Immunostaining was performed on 5μm paraffin sections for osteocalcin (OCN) and BrdU or 10μm frozen non-decalcified sections for perilipin (PLIN). For OCN and BrdU immunostaining, antigen retrieval was performed by incubating tissue sections in 10μg/ml proteinase K for 10 minutes followed by incubation in 3% H_2O_2 (v/v in Methanol) for 10 minutes to block endogenous peroxidase activity. Antibodies against BrdU (RRID:AB_10986341, 1:1000 dilution), OCN (RRID:AB_1587337, 1:500 dilution) or Perilipin (RRID:AB_10829911, 1:200 dilution) were used. TUNEL staining was performed using the in-situ Cell Death Detection Kit, Fluorescein. All Image analysis was performed in a blinded and coded manner.

Cell culture—Primary bone marrow skeletal stem cells (SSC) were isolated as follows. Briefly, the diaphyses of the femur and tibiae were isolated and all extemporaneous tissue was removed. The epiphyses were removed and marrow was collected by centrifugation. Red blood cells were lysed and cells were washed one time before plating. For colony forming efficiency assays, 1×10^6 SSC were plated in a T25 flask. 3 hours after plating, non-adherent cells were removed by washing vigorously with media. Cells were then cultured for 14 days as indicated for CFU-F and CFU-Ap assays. After 14 days, colonies were switch to

either adipogenic media (CFU-Ad) or osteogenic media (CFU-Ob) for an additional 14 days. For high density cultures, SSC were plated and washed after 3 and 6 days to remove non-adherent cells. SSC were passaged at day 7 and all experiments were carried out at a seeding density of 21,000 cells/cm^2. Osteoblast differentiation was initiated when cells were 95% confluent by replacing the medium with α-MEM supplemented with 50 mg/ml ascorbic acid and 10 mM β-glycerophosphate for the indicated time period with a change of media every 48 hours. Mineralization was assessed by von Kossa or alizarin red staining. Alkaline phosphatase staining was performed using the one-step nitro-blue tetrazolium (NBT) and 5-bromo-4-chloro-3'-indolyphosphate p-toluidine salt (BCIP) solution. Adipocyte differentiation was initiated 3 days after cells reached confluency by replacing the medium with α-MEM supplemented with 1.7μM Insulin, 1μM Dexamethasone and 0.5 mM IBMX for three days. Media was then replaced with α-MEM supplemented with 1.7μM Insulin only for 4 days with a change of media every 48 hours. Adipogenic media for CFU-Ad assays also contained 1μM Rosiglitazone. Lipid droplets were visualized by Oil Red O staining. In the indicated experiments, glutamine free α-MEM was supplemented with 2mM L-glutamine, 10μM BPTES, 200μM O-(carboxymethyl)hydroxylamine hemihdrate (AOA), 7.5μM Bithionol, 1mM glutathione reduced ethyl ester, or 1mM dimethyl α-KG.

Mass Spectrometry analysis of glutamine metabolism—SSC were cultured to confluency in 6cm plates prior to initiation of treatment. SSC were either treated with BPTES for 1 hour or were cultured for 7 days in either growth media or osteogenic media prior to incubation in 2mM [U-^{13}C]glutamine for up to one hour. At the end of the incubation, cells were washed with cold PBS and extracted 3 times with −80˚C methanol on dry ice. The methanol extract was spiked with 20 nmol norvaline as an internal standard and centrifuged at 2000 × g force for 30 minutes after vortex. The supernatant was completely dried by N_2 gas. A modified GC-MS method was used for small polar metabolites assay (Wang, et al., 2018). The dried residues were resuspended in 25 μL of methoxylamine hydrochloride (2% (w/v) in pyridine) and incubated at 40°C for ninety minutes on a heating block. After brief centrifugation, 35 μL of MTBSTFA + 1% TBDMS was added, and the samples were incubated at 60°C for thirty minutes. The derivatized samples were centrifuged for five minutes at 20000 × g, and the supernatants were transferred to GC vials for GC-MS analysis. The injection volume was 1 μL, and samples were injected in split or splitless mode depending on analyte of interest. GC oven temperature was held at 80°C for two minutes, increased to 280°C at 7°C/min, and held at 280°C for a total run time of forty minutes.

GC-MS analysis was performed on an Agilent 7890B GC system equipped with a HP-5MS capillary column (30 m, 0.25 mm i.d., 0.25 μm-phase thickness; Agilent J&W Scientific), connected to an Agilent 5977A Mass Spectrometer operating under ionization by electron impact (Meister) at 70 eV. Helium flow was maintained at 1 mL/min. The source temperature was maintained at 230°C, the MS quad temperature at 150°C, the interface temperature at 280°C, and the inlet temperature at 250°C. Mass spectra were recorded in selected ion monitoring (SIM) mode with 4 ms dwell time.

GSH and GSSG labeling analysis by LC-MS/MS—The method was modified from our previous LC-MS/MS method (Kombu, et al., 2009). Cell pellet samples were treated with 10 mM N-Ethylmaleimide (NEM), sonicated for 1 minute, then add 250 ul MeOH, centrifuge for 15 minutes, dry the samples completely. Redissolve the dried residue in 50 ul H_2O and transferred to LC-MS vials for analysis.

A Sciex QTRAP 6500+ (Sciex, Ontario, Canada) equipped with trubo elextrospray ion source was operated under positive ionization mode. The UPLC system consisted of an ExionLC AD autosampler, a column oven, and gradient pumps. A Phenomenex Aeris PEPTIDE 1.7 uM XB-C18 column (50×2.1 mm, Torrance, CA) was selected for GSH and GSSG separation. The column was kept at 45°C. The GSSG and GSH were separated by a gradient elution. Mobile phase A was 0.1% formic acid in water-acetonitrile (98:2, vol/vol), and mobile phase B was 0.1% formic acid in acetonitrile-water (98:2, vol/vol). The flow rate was 0.4 ml/min.

Glutaminase activity assay—Primary cells cultured to confluency were incubated in α-MEM media containing 5mM glucose and 2mM glutamine for 12 hours prior to the experiment. Cells were washed 3 times with Hanks Buffered Saline Solution (HBSS) and cultured for 20 minutes in α-MEM media containing 5mM glucose, 2μM Glutamine and 4 μCi/mL L (2,3,4-^{3}H)-Glutamine. Glutaminase activity was terminated by washing 3 times with ice cold HBSS and scraping cells in 1mL ice cold milliQ water. Cells were lysed by sonication for 1 minute with 1 second pulses at 20% amplitude. After clarification, cell lysates were bound onto AG 1-X8 polyprep anion exchange columns. Uncharged glutamine was eluted with three 2mL volumes of water. Glutamate and downstream metabolites were eluted with three 2mL volumes of 0.1M HCl. Eluent fractions were pooled and combined with 4mL scintillation cocktail and DPM was measured using a Beckman LS6500 Scintillation counter.

RNA isolation and qPCR—Total RNA was isolated from cultured cells using the RNAeasy kit with on-column DNase treatment. Reverse transcription was performed using 400ng total RNA with the iScript cDNA synthesis kit. Reactions were set up in technical and biological triplicates in a 96 well format on an ABI QuantStudio 3, using SYBR green chemistry. The PCR conditions were 95°C for 3 min followed by 40 cycles of 95°C for 10s and 60°C for 30s. Gene expression was normalized to *Actb* mRNA and relative expression was calculated using the $2^{-(\Delta\Delta Ct)}$ method. Primers were used at 0.1 μM, and their sequences are listed in Table S4. PCR efficiency was optimized and melting curve analyses of products were performed to ensure reaction specificity.

Western blotting—Cells were scraped in lysis buffer containing 50 mM Tris (pH 7.4), 15 mM NaCl, 0.5% NP-40, and a protease inhibitor mix. Protein concentration was estimated by the BCA method. Protein (20 μg) was resolved on 4–15% polyacrylamide gel and subjected to immunoblot analyses using the following antibodies. Antibodies against GLS (RRID:AB_2110382), Cyclin D1, (RRID:AB_2228523), Cyclin D3 (RRID:AB_2070801), α-tubulin (RRID:AB_2210548), AMPK (RRID:AB_330331), P-T172 AMPK (RRID:AB_330330), Eif2α (RRID:AB_10692650), PS51 Eif2α (RRID:AB_2096481), Chop (RRID:AB_2089254), Atf4 (RRID:AB_2058752) and β-actin (RRID:AB_330288)

were used to detect the respective protein levels. All primary antibodies were diluted 1:1000 in blocking solution (5% milk, 0.1% Tween in TBS). The immunoblots were blocked for one hour at room temperature in 5% milk (TBS, 0.1% Tween) followed by an overnight incubation at 4°C in their respective diluted primary antibody solutions. Membranes were then washed three times using TBS/Tween 0.1% and further incubated with the secondary antibody, HRP goat anti-rabbit (RRID:AB_2099233) or HRP anti-mouse (RRID:AB_330924) in 5% milk (TBS/Tween 0.1%) for 1 hour at room temperature. All secondary antibodies were diluted 1:2000 in blocking solution. All blots were developed using either the Clarity ECL substrate or the SuperSignal West Femto substrate. Each experiment was repeated for a minimum of three times with three independently prepared protein samples.

QUANTIFICATION AND STATISTICAL ANALYSIS

Statistical analyses were performed using Graphpad Prism 6 software. All data are shown as mean values ±SD. In cell culture studies, statistical significance was determined by an unpaired 2-tailed Student's *t*-test. For uCT and CFU studies statistical significance was determine by a paired 2-tailed Student's *t*-test comparing paired littermate controls. Data were normally distributed as determined using the Komogorov-Smirnov test. A P value of less than 0.05 is considered statistically significant. Statistical parameters, including the value of n, are noted in the figure legends. Unless otherwise noted, all experiments were performed on 3 individual samples.

Supplementary Material

Refer to Web version on PubMed Central for supplementary material.

Acknowledgements:

The authors thank Drs. Thomas Carroll and Ryan Gray for critical comments on this manuscript. This work was supported by National Institute of Health R01 grants (2AR063071) to MJH and (AR071967) to CMK.

References:

(2004). In Bone Health and Osteoporosis: A Report of the Surgeon General, (Rockville (MD).

Almeida M, Han L, Martin-Millan M, O'Brien CA, and Manolagas SC (2007). Oxidative stress antagonizes Wnt signaling in osteoblast precursors by diverting beta-catenin from T cell factor- to forkhead box O-mediated transcription. J Biol Chem 282, 27298–305.

Bai XC, Lu D, Bai J, Zheng H, Ke ZY, Li XM, and Luo SQ (2004). Oxidative stress inhibits osteoblastic differentiation of bone cells by ERK and NF-kappaB. Biochem Biophys Res Commun 314, 197–207. [PubMed: 14715266]

Balani DH, Ono N, and Kronenberg HM (2017). Parathyroid hormone regulates fates of murine osteoblast precursors in vivo. J Clin Invest 127, 3327–3338. [PubMed: 28758904]

Becker DJ, Kilgore ML, and Morrisey MA (2010). The societal burden of osteoporosis. Curr Rheumatol Rep 12, 186–91. [PubMed: 20425518]

Bianco P, and Robey PG (2015). Skeletal stem cells. Development 142, 1023–7. [PubMed: 25758217]

Birsoy K, Wang T, Chen WW, Freinkman E, Abu-Remaileh M, and Sabatini DM (2015). An Essential Role of the Mitochondrial Electron Transport Chain in Cell Proliferation Is to Enable Aspartate Synthesis. Cell 162, 540–51. [PubMed: 26232224]

Borle AB, Nichols N, and Nichols G Jr. (1960). Metabolic studies of bone in vitro. I. Normal bone. J Biol Chem 235, 1206–10. [PubMed: 13802861]

Chen CT, Shih YR, Kuo TK, Lee OK, and Wei YH (2008). Coordinated changes of mitochondrial biogenesis and antioxidant enzymes during osteogenic differentiation of human mesenchymal stem cells. Stem Cells 26, 960–8. [PubMed: 18218821]

Colombo SL, Palacios-Callender M, Frakich N, Carcamo S, Kovacs I, Tudzarova S, and Moncada S. (2011). Molecular basis for the differential use of glucose and glutamine in cell proliferation as revealed by synchronized HeLa cells. Proc Natl Acad Sci U S A 108, 21069–74.

D'Ippolito G, Schiller PC, Ricordi C, Roos BA, and Howard GA (1999). Age-related osteogenic potential of mesenchymal stromal stem cells from human vertebral bone marrow. J Bone Miner Res 14, 1115–22. [PubMed: 10404011]

DeBerardinis RJ, Mancuso A, Daikhin E, Nissim I, Yudkoff M, Wehrli S, and Thompson CB (2007). Beyond aerobic glycolysis: transformed cells can engage in glutamine metabolism that exceeds the requirement for protein and nucleotide synthesis. Proc Natl Acad Sci U S A 104, 19345–50.

DeFalco J, Tomishima M, Liu H, Zhao C, Cai X, Marth JD, Enquist L, and Friedman JM (2001). Virus-assisted mapping of neural inputs to a feeding center in the hypothalamus. Science 291, 2608–13. [PubMed: 11283374]

Ding L, and Morrison SJ (2013). Haematopoietic stem cells and early lymphoid progenitors occupy distinct bone marrow niches. Nature 495, 231–5. [PubMed: 23434755]

Eagle H. (1955). Nutrition needs of mammalian cells in tissue culture. Science 122, 501–14. [PubMed: 13255879]

Eagle H, Oyama VI, Levy M, Horton CL, and Fleischman R. (1956). The growth response of mammalian cells in tissue culture to L-glutamine and L-glutamic acid. J Biol Chem 218, 607–16. [PubMed: 13295214]

Egan KP, Brennan TA, and Pignolo RJ (2012). Bone histomorphometry using free and commonly available software. Histopathology 61, 1168–73. [PubMed: 22882309]

Eisman JA, Bogoch ER, Dell R, Harrington JT, McKinney RE Jr., McLellan A, Mitchell PJ, Silverman S, Singleton R, Siris E, et al. (2012). Making the first fracture the last fracture: ASBMR task force report on secondary fracture prevention. J Bone Miner Res 27, 2039–46. [PubMed: 22836222]

Fairfield H, Falank C, Harris E, Demambro V, McDonald M, Pettitt JA, Mohanty ST, Croucher P, Kramer I, Kneissel M, et al. (2018). The skeletal cell-derived molecule sclerostin drives bone marrow adipogenesis. J Cell Physiol 233, 1156–1167. [PubMed: 28460416]

Fan Y, Hanai JI, Le PT, Bi R, Maridas D, DeMambro V, Figueroa CA, Kir S, Zhou X, Mannstadt M, et al. (2017). Parathyroid Hormone Directs Bone Marrow Mesenchymal Cell Fate. Cell Metab 25, 661–672. [PubMed: 28162969]

Friedenstein AJ, Piatetzky S II, and Petrakova KV (1966). Osteogenesis in transplants of bone marrow cells. J Embryol Exp Morphol 16, 381–90. [PubMed: 5336210]

Greenbaum A, Hsu YM, Day RB, Schuettpelz LG, Christopher MJ, Borgerding JN, Nagasawa T, and Link DC (2013). CXCL12 in early mesenchymal progenitors is required for haematopoietic stem-cell maintenance. Nature 495, 227–30. [PubMed: 23434756]

Guntur AR, Le PT, Farber CR, and Rosen CJ (2014). Bioenergetics during calvarial osteoblast differentiation reflect strain differences in bone mass. Endocrinology 155, 1589–95. [PubMed: 24437492]

Huang H, Vandekeere S, Kalucka J, Bierhansl L, Zecchin A, Bruning U, Visnagri A, Yuldasheva N, Goveia J, Cruys B, et al. (2017). Role of glutamine and interlinked asparagine metabolism in vessel formation. EMBO J 36, 2334–2352. [PubMed: 28659375]

Ito K, Carracedo A, Weiss D, Arai F, Ala U, Avigan DE, Schafer ZT, Evans RM, Suda T, Lee CH, et al. (2012). A PML-PPAR-delta pathway for fatty acid oxidation regulates hematopoietic stem cell maintenance. Nat Med 18, 1350–8. [PubMed: 22902876]

Justesen J, Stenderup K, Ebbesen EN, Mosekilde L, Steiniche T, and Kassem M. (2001). Adipocyte tissue volume in bone marrow is increased with aging and in patients with osteoporosis. Biogerontology 2, 165–71. [PubMed: 11708718]

Karner CM, Esen E, Chen J, Hsu FF, Turk J, and Long F. (2016). Wnt Protein Signaling Reduces Nuclear Acetyl-CoA Levels to Suppress Gene Expression during Osteoblast Differentiation. J Biol Chem 291, 13028–39.

Karner CM, Esen E, Okunade AL, Patterson BW, and Long F. (2015). Increased glutamine catabolism mediates bone anabolism in response to WNT signaling. J Clin Invest 125, 551–62. [PubMed: 25562323]

Kauppinen RA, Sihra TS, and Nicholls DG (1987). Aminooxyacetic acid inhibits the malate-aspartate shuttle in isolated nerve terminals and prevents the mitochondria from utilizing glycolytic substrates. Biochim Biophys Acta 930, 173–8. [PubMed: 3620514]

Kim B, Li J, Jang C, and Arany Z. (2017). Glutamine fuels proliferation but not migration of endothelial cells. EMBO J 36, 2321–2333. [PubMed: 28659379]

Knobloch M, Braun SM, Zurkirchen L, von Schoultz C, Zamboni N, Arauzo-Bravo MJ, Kovacs WJ, Karalay O, Suter U, Machado RA, et al. (2013). Metabolic control of adult neural stem cell activity by Fasn-dependent lipogenesis. Nature 493, 226–30. [PubMed: 23201681]

Komarova SV, Ataullakhanov FI, and Globus RK (2000). Bioenergetics and mitochondrial transmembrane potential during differentiation of cultured osteoblasts. Am J Physiol Cell Physiol 279, C1220–9.

Kombu RS, Zhang GF, Abbas R, Mieyal JJ, Anderson VE, Kelleher JK, Sanabria JR, and Brunengraber H. (2009). Dynamics of glutathione and ophthalmate traced with 2H-enriched body water in rats and humans. Am J Physiol Endocrinol Metab 297, E260–9. [PubMed: 19401458]

Korangath P, Teo WW, Sadik H, Han L, Mori N, Huijts CM, Wildes F, Bharti S, Zhang Z, Santa-Maria CA, et al. (2015). Targeting Glutamine Metabolism in Breast Cancer with Aminooxyacetate. Clin Cancer Res 21, 3263–73. [PubMed: 25813021]

Le A, Lane AN, Hamaker M, Bose S, Gouw A, Barbi J, Tsukamoto T, Rojas CJ, Slusher BS, Zhang H, et al. (2012). Glucose-independent glutamine metabolism via TCA cycling for proliferation and survival in B cells. Cell Metab 15, 110–21. [PubMed: 22225880]

Lecka-Czernik B, Stechschulte LA, Czernik PJ, Sherman SB, Huang S, and Krings A. (2017). Marrow Adipose Tissue: Skeletal Location, Sexual Dimorphism, and Response to Sex Steroid Deficiency. Front Endocrinol (Lausanne) 8, 188. [PubMed: 28824548]

Li J, Zhang N, Huang X, Xu J, Fernandes JC, Dai K, and Zhang X. (2013). Dexamethasone shifts bone marrow stromal cells from osteoblasts to adipocytes by C/EBPalpha promoter methylation. Cell Death Dis 4, e832.

Li M, Smith CJ, Walker MT, and Smith TJ (2009). Novel inhibitors complexed with glutamate dehydrogenase: allosteric regulation by control of protein dynamics. J Biol Chem 284, 22988–3000.

Logan M, Martin JF, Nagy A, Lobe C, Olson EN, and Tabin CJ (2002). Expression of Cre Recombinase in the developing mouse limb bud driven by a Prxl enhancer. Genesis 33, 77–80. [PubMed: 12112875]

Masson J, Darmon M, Conjard A, Chuhma N, Ropert N, Thoby-Brisson M, Foutz AS, Parrot S, Miller GM, Jorisch R, et al. (2006). Mice lacking brain/kidney phosphate-activated glutaminase have impaired glutamatergic synaptic transmission, altered breathing, disorganized goal-directed behavior and die shortly after birth. J Neurosci 26, 4660–71. [PubMed: 16641247]

McDonough MA, Loenarz C, Chowdhury R, Clifton IJ, and Schofield CJ (2010). Structural studies on human 2-oxoglutarate dependent oxygenases. Curr Opin Struct Biol 20, 659–72. [PubMed: 20888218]

Meister A. (1975). Function of glutathione in kidney via the gamma-glutamyl cycle. Med Clin North Am 59, 649–66. [PubMed: 236410]

Metallo CM, Gameiro PA, Bell EL, Mattaini KR, Yang J, Hiller K, Jewell CM, Johnson ZR, Irvine DJ, Guarente L, et al. (2011). Reductive glutamine metabolism by IDH1 mediates lipogenesis under hypoxia. Nature 481, 380–4. [PubMed: 22101433]

Mizoguchi T, Pinho S, Ahmed J, Kunisaki Y, Hanoun M, Mendelson A, Ono N, Kronenberg HM, and Frenette PS (2014). Osterix marks distinct waves of primitive and definitive stromal progenitors during bone marrow development. Dev Cell 29, 340–9. [PubMed: 24823377]

Mody N, Parhami F, Sarafian TA, and Demer LL (2001). Oxidative stress modulates osteoblastic differentiation of vascular and bone cells. Free Radic Biol Med 31, 509–19. [PubMed: 11498284]

Moerman EJ, Teng K, Lipschitz DA, and Lecka-Czernik B. (2004). Aging activates adipogenic and suppresses osteogenic programs in mesenchymal marrow stroma/stem cells: the role of PPAR-gamma2 transcription factor and TGF-beta/BMP signaling pathways. Aging Cell 3, 379–89. [PubMed: 15569355]

Mullen AR, Wheaton WW, Jin ES, Chen PH, Sullivan LB, Cheng T, Yang Y, Linehan WM, Chandel NS, and DeBerardinis RJ (2011). Reductive carboxylation supports growth in tumour cells with defective mitochondria. Nature 481, 385–8. [PubMed: 22101431]

Nishida S, Endo N, Yamagiwa H, Tanizawa T, and Takahashi HE (1999). Number of osteoprogenitor cells in human bone marrow markedly decreases after skeletal maturation. J Bone Miner Metab 17, 171–7. [PubMed: 10757676]

Oburoglu L, Tardito S, Fritz V, de Barros SC, Merida P, Craveiro M, Mamede J, Cretenet G, Mongellaz C, An X, et al. (2014). Glucose and glutamine metabolism regulate human hematopoietic stem cell lineage specification. Cell Stem Cell 15, 169–84. [PubMed: 24953180]

Owen M, and Friedenstein AJ (1988). Stromal stem cells: marrow-derived osteogenic precursors. Ciba Found Symp 136, 42–60. [PubMed: 3068016]

Park D, Spencer JA, Koh BI, Kobayashi T, Fujisaki J, Clemens TL, Lin CP, Kronenberg HM, and Scadden DT (2012). Endogenous bone marrow MSCs are dynamic, fate-restricted participants in bone maintenance and regeneration. Cell Stem Cell 10, 259–72. [PubMed: 22385654]

Scheller EL, Troiano N, Vanhoutan JN, Bouxsein MA, Fretz JA, Xi Y, Nelson T, Katz G, Berry R, Church CD, et al. (2014). Use of osmium tetroxide staining with microcomputerized tomography to visualize and quantify bone marrow adipose tissue in vivo. Methods Enzymol 537, 123–39. [PubMed: 24480344]

Schofield CJ, and Zhang Z. (1999). Structural and mechanistic studies on 2-oxoglutarate-dependent oxygenases and related enzymes. Curr Opin Struct Biol 9, 722–31. [PubMed: 10607676]

Stein WH, and Moore S. (1954). The free amino acids of human blood plasma. J Biol Chem 211, 915–26. [PubMed: 13221597]

Still ER, and Yuneva MO (2017). Hopefully devoted to Q: targeting glutamine addiction in cancer. Br J Cancer 116, 1375–1381. [PubMed: 28441384]

Sullivan LB, Gui DY, Hosios AM, Bush LN, Freinkman E, and Vander Heiden MG (2015). Supporting Aspartate Biosynthesis Is an Essential Function of Respiration in Proliferating Cells. Cell 162, 552–63. [PubMed: 26232225]

Thangavelu K, Pan CQ, Karlberg T, Balaji G, Uttamchandani M, Suresh V, Schuler H, Low BC, and Sivaraman J. (2012). Structural basis for the allosteric inhibitory mechanism of human kidney-type glutaminase (KGA) and its regulation by Raf-Mek-Erk signaling in cancer cell metabolism. Proc Natl Acad Sci U S A 109, 7705–10. [PubMed: 22538822]

Tormos KV, Anso E, Hamanaka RB, Eisenbart J, Joseph J, Kalyanaraman B, and Chandel NS (2011). Mitochondrial complex III ROS regulate adipocyte differentiation. Cell Metab 14, 537–44. [PubMed: 21982713]

Velletri T, Romeo F, Tucci P, Peschiaroli A, Annicchiarico-Petruzzelli M, Niklison-Chirou MV, Amelio I, Knight RA, Mak TW, Melino G, et al. (2013). GLS2 is transcriptionally regulated by p73 and contributes to neuronal differentiation. Cell Cycle 12, 3564–73. [PubMed: 24121663]

Wang W, Zhang Y, Lu W, and Liu K. (2015). Mitochondrial reactive oxygen species regulate adipocyte differentiation of mesenchymal stem cells in hematopoietic stress induced by arabinosylcytosine. PLoS One 10, e0120629.

Wang Y, Christopher BA, Wilson KA, Muoio D, McGarrah RW, Brunengraber H, and Zhang GF (2018). Propionate-induced changes in cardiac metabolism, notably CoA trapping, are not altered by l-carnitine. Am J Physiol Endocrinol Metab 315, E622–E633. [PubMed: 30016154]

Wise DR, and Thompson CB (2010). Glutamine addiction: a new therapeutic target in cancer. Trends Biochem Sci 35, 427–33. [PubMed: 20570523]

Wise DR, Ward PS, Shay JE, Cross JR, Gruber JJ, Sachdeva UM, Platt JM, DeMatteo RG, Simon MC, and Thompson CB (2011). Hypoxia promotes isocitrate dehydrogenase-dependent carboxylation

of alpha-ketoglutarate to citrate to support cell growth and viability. Proc Natl Acad Sci U S A 108, 19611–6.

Wu M, Wang Y, Shao JZ, Wang J, Chen W, and Li YP (2017). Cbfbeta governs osteoblast-adipocyte lineage commitment through enhancing beta-catenin signaling and suppressing adipogenesis gene expression. Proc Natl Acad Sci U S A 114, 10119–10124.

Yang R, Yu T, Kou X, Gao X, Chen C, Liu D, Zhou Y, and Shi S. (2018). Tet1 and Tet2 maintain mesenchymal stem cell homeostasis via demethylation of the P2rX7 promoter. Nat Commun 9, 2143. [PubMed: 29858571]

Yue R, Zhou BO, Shimada IS, Zhao Z, and Morrison SJ (2016). Leptin Receptor Promotes Adipogenesis and Reduces Osteogenesis by Regulating Mesenchymal Stromal Cells in Adult Bone Marrow. Cell Stem Cell 18, 782–96. [PubMed: 27053299]

Zhang J, Pavlova NN, and Thompson CB (2017). Cancer cell metabolism: the essential role of the nonessential amino acid, glutamine. EMBO J 36, 1302–1315. [PubMed: 28420743]

Zhang M, Xuan S, Bouxsein ML, von Stechow D, Akeno N, Faugere MC, Malluche H, Zhao G, Rosen CJ, Efstratiadis A, et al. (2002). Osteoblast-specific knockout of the insulin-like growth factor (IGF) receptor gene reveals an essential role of IGF signaling in bone matrix mineralization. J Biol Chem 277, 44005–12.

Zhou BO, Yue R, Murphy MM, Peyer JG, and Morrison SJ (2014). Leptin-receptor-expressing mesenchymal stromal cells represent the main source of bone formed by adult bone marrow. Cell Stem Cell 15, 154–68. [PubMed: 24953181]

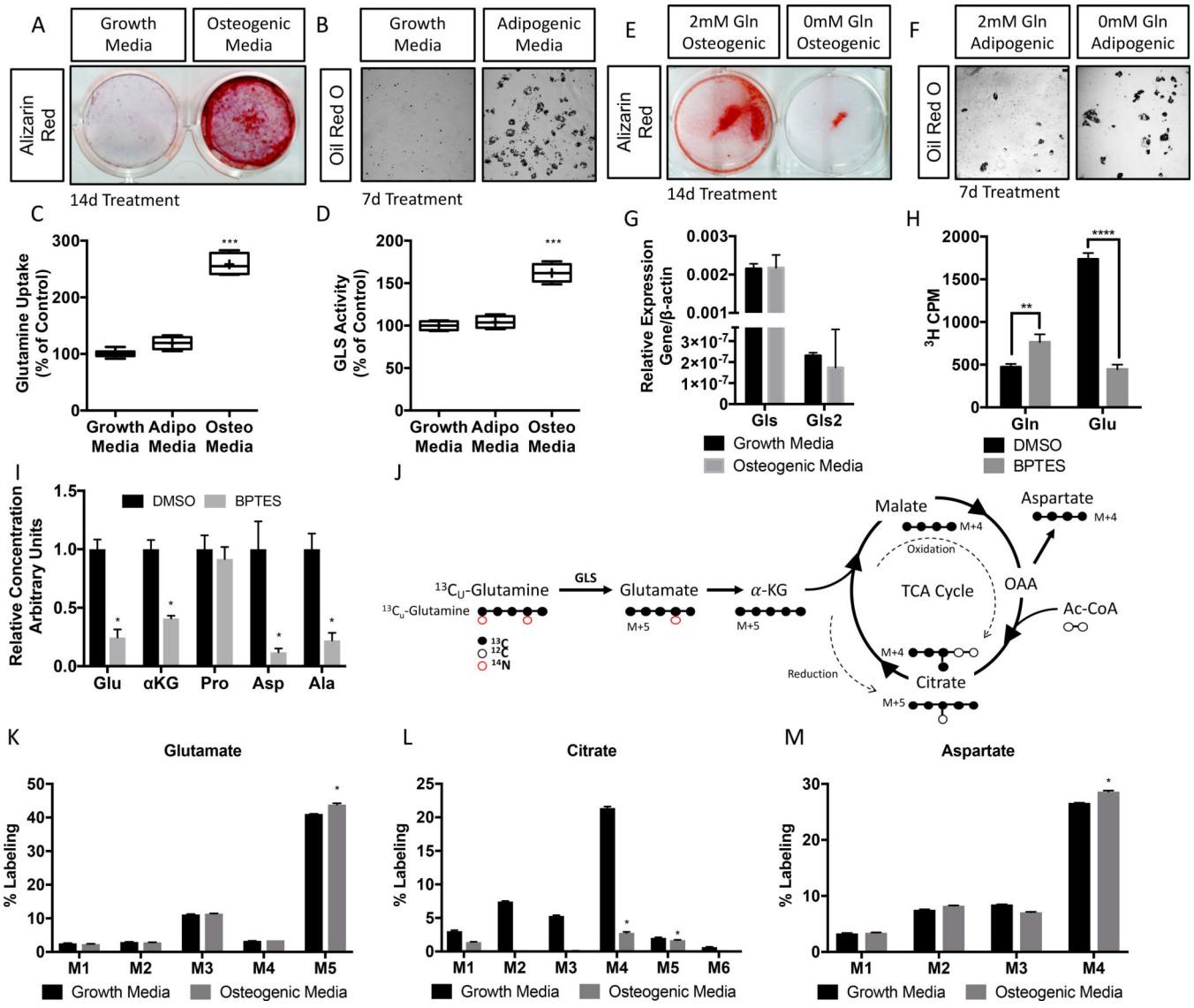

Figure 1: Skeletal stem cells increase glutamine consumption and metabolism during osteoblast differentiation.

(A) Alizarin Red staining of SSC induced to undergo osteoblast differentiation for 14 days. **(B)** Oil Red O staining of SSC induced to undergo adipocyte differentiation for 7 days. **(C-D)** Tukey box and whisker plot of measurements of glutamine uptake **(C)** or GLS activity **(D)** in SSC after 7 days of differentiation. Median and mean are represented by the line and cross respectively. n=5. **(E-F)** Effect of glutamine withdrawal on osteoblast **(E)** or adipocyte **(F)** differentiation in SSC. **(G)** RT-qPCR analyses of gene expression in SSC cultured for 7 days in osteogenic media. **(H)** Effect of BPTES on GLS activity in SSC. **(I)** Effect of BPTES on metabolite concentration measured by mass spectrometry. **(J)** Graphical depiction of tracing glutamine metabolism using [U-^{13}C]glutamine). Black filled circles indicate ^{13}C whereas black open circles and red open circles denote ^{12}C and ^{14}N respectively. OAA – oxaloacetate, αKG – α-ketoglutarate, ac-CoA – Acetyl-CoA. **(K-M)**

Fractional contribution of [U-^{13}C]glutamine to glutamate **(K)**, citrate **(L)**, and aspartate **(M)**. **p≤0.005, ***p≤0.0005, ****p≤0.00005. See also Figure S1.

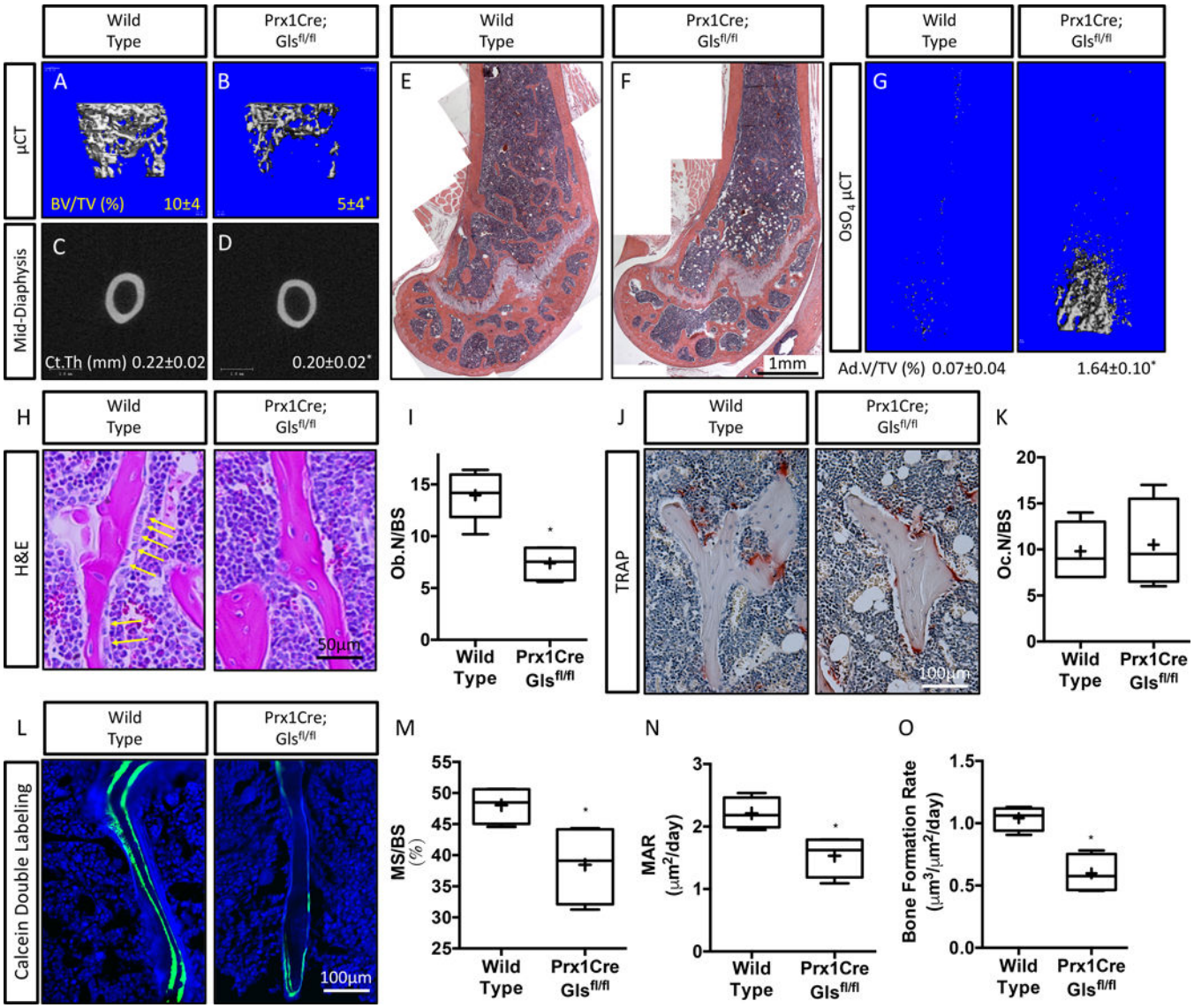

Figure 2: *Gls* ablation reduces bone mass *in vivo*.

(A-D) Representative µCT images of a 4-month old *Prx1Cre;Gls*$^{fl/+}$ (Wild Type) or *Prx1Cre;Gls*$^{fl/fl}$ mutant mouse. BV/TV – Bone volume/Tissue Volume. Ct.Th – Cortical Thickness. **(E-F)** Representative H&E stained distal femur of 4-month female mice. **(G)** Representative OsO_4 µCT images of a 4-month old female mice. Ad.V/TV – Adipose volume/tissue volume. **(H)** Representative H&E stained section used to quantify osteoblasts (arrows). **(I)** Tukey box and whisker plot of the quantification of osteoblast numbers (Ob.N) per bone surface. **(J)** Representative TRAP stained section used to quantify osteoclast numbers. **(K)** Tukey box and whisker plot of the quantification of osteoclast numbers (Oc.N) per bone surface. **(L)** Representative calcein double labeled sections of the distal femur from 4-month old mice. **(M-O)** Tukey box and whisker plots of the quantification of mineralized surface per bone surface (MS/BS) **(M)**, mineral apposition rate MAR **(N)**, or bone formation rate (BFR) **(O)** derived from calcein double labeling. Median and mean are represented by the line and cross respectively. N=5. *p≤0.05. See also Figure S2 and Table S1.

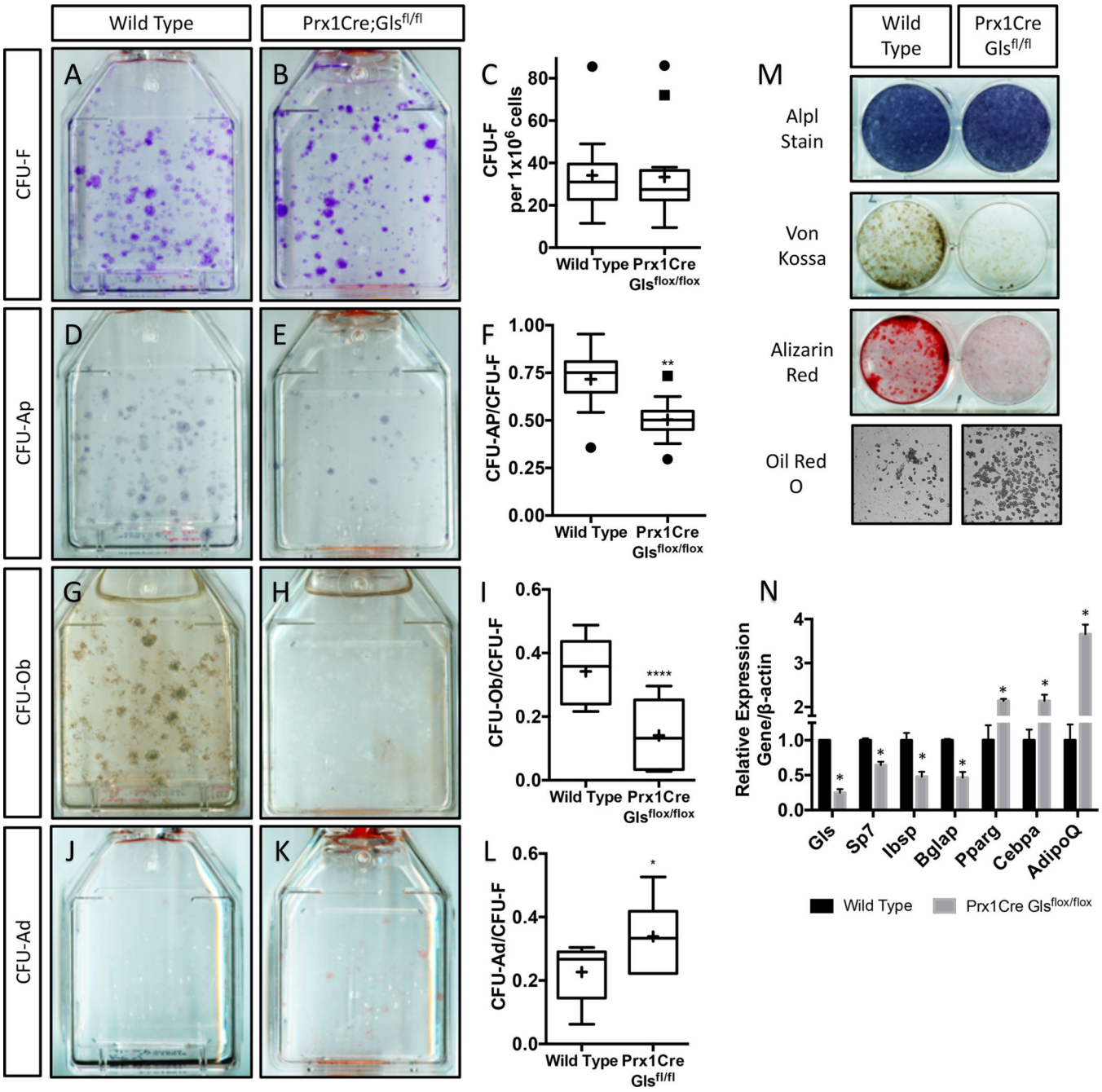

Figure 3: *Gls* is required for osteoblast specification and differentiation from SSC.

Representative images and quantification of colony forming unit (CFU) assays stained with Crystal Violet **(A-C)**, alkaline phosphatase **(D-F)**, Von Kossa **(G-I)**, or Oil Red O **(J-L)**. **(C, F, I, L)** Tukey box and whisker plots displaying colonies containing at least 50 cells. n=13 or 14 for wild type or *Prx1Cre;Gls*$^{fl/fl}$ respectively . **(M)** Functional assays or RT-qPCR **(N)** analyses of the effect of *Gls* deletion on cell fate decision in primary SSC cultured in osteogenic and adipogenic media for 14 days. n=4 mice. *p≤0.05, **p≤0.005, ****p≤0.00005. See also Figure S3.

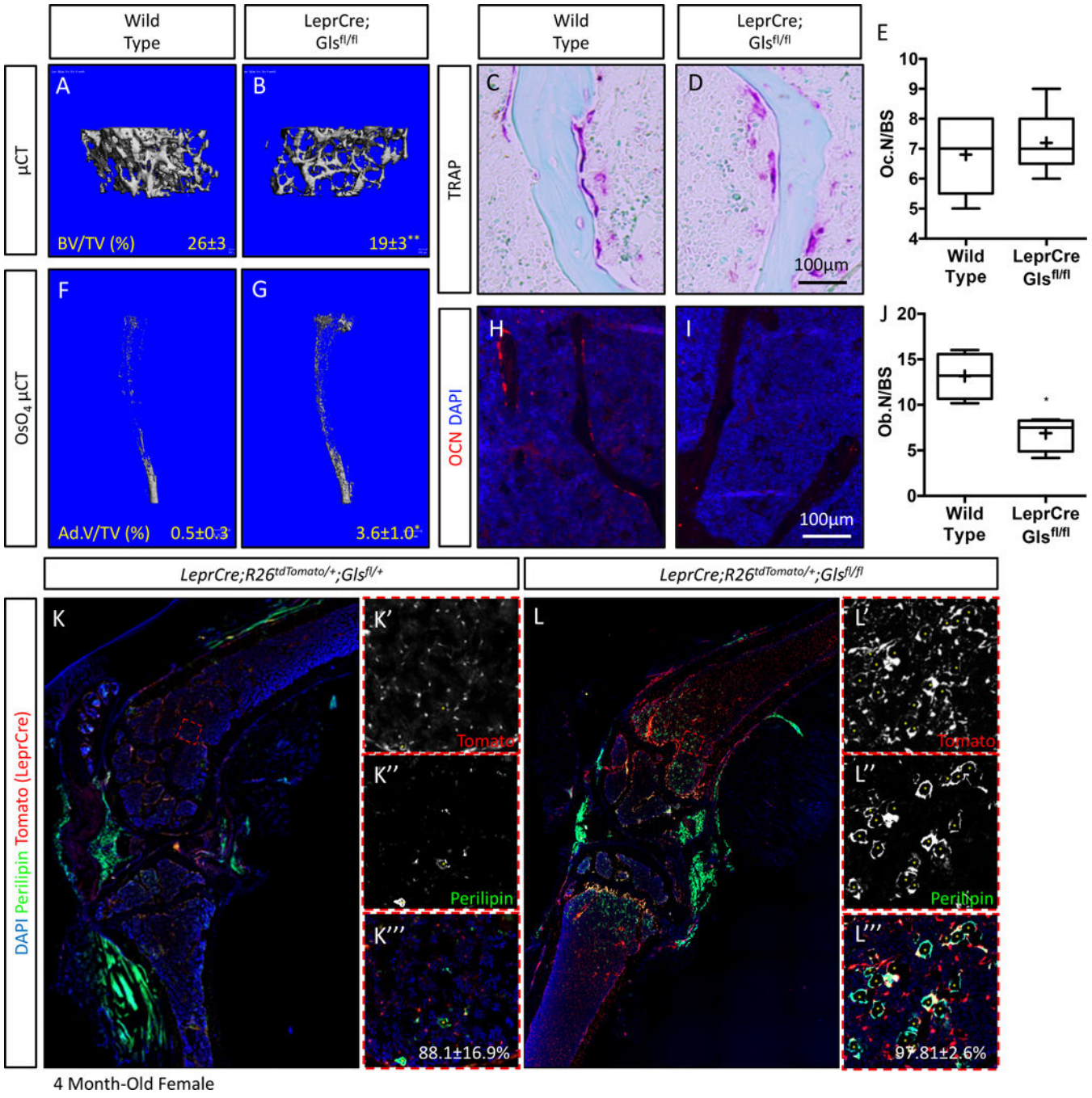

Figure 4: *Gls* acts in SSC to regulate lineage allocation.

(A-B) Representative µCT image of trabecular bone from a 4-month old *LeprCre;Gls*$^{fl/+}$ (Wild Type) or *LeprCre;Gls*$^{fl/fl}$ mutant mouse. BV/TV – Bone Volume/Tissue Volume. **(C-D)** Representative TRAP stained section used to quantify osteoclast numbers. **(E)** Tukey box and whisker plot of the quantification of osteoclast numbers (Oc.N) per bone surface. **(F-G)** Representative OsO_4 µCT images of the tibia from 4-month old mice. Ad.V/TV – Adipose volume/tissue volume. n=8 or 12 for wild type or *LeprCre;Gls*$^{fl/fl}$ respectively. **(H-J)** Representative immunofluorescent staining for Osteocalcin (OCN) used to quantify

osteoblast numbers (Ob.N/BS) in **(J)**. **(K)** Anti-Perilipin (PLIN) and anti-tomato immunofluorescent staining of 4 month old *LeprCre;R26*$^{tdTomato/+}$*;Gls*$^{fl/+}$ (Wild type) or *LeprCre;R26*$^{tdTomato/+}$*;Gls*$^{fl/fl}$ hindlimbs. Inset images of boxed region show individual channels (K', K'', K''', L', L'', L'''). Quantification of PLIN, tomato double positive cells shown in (K''' and L'''). n=3. *p≤0.05, Student's t test. See also Figure S4 and Table S3.

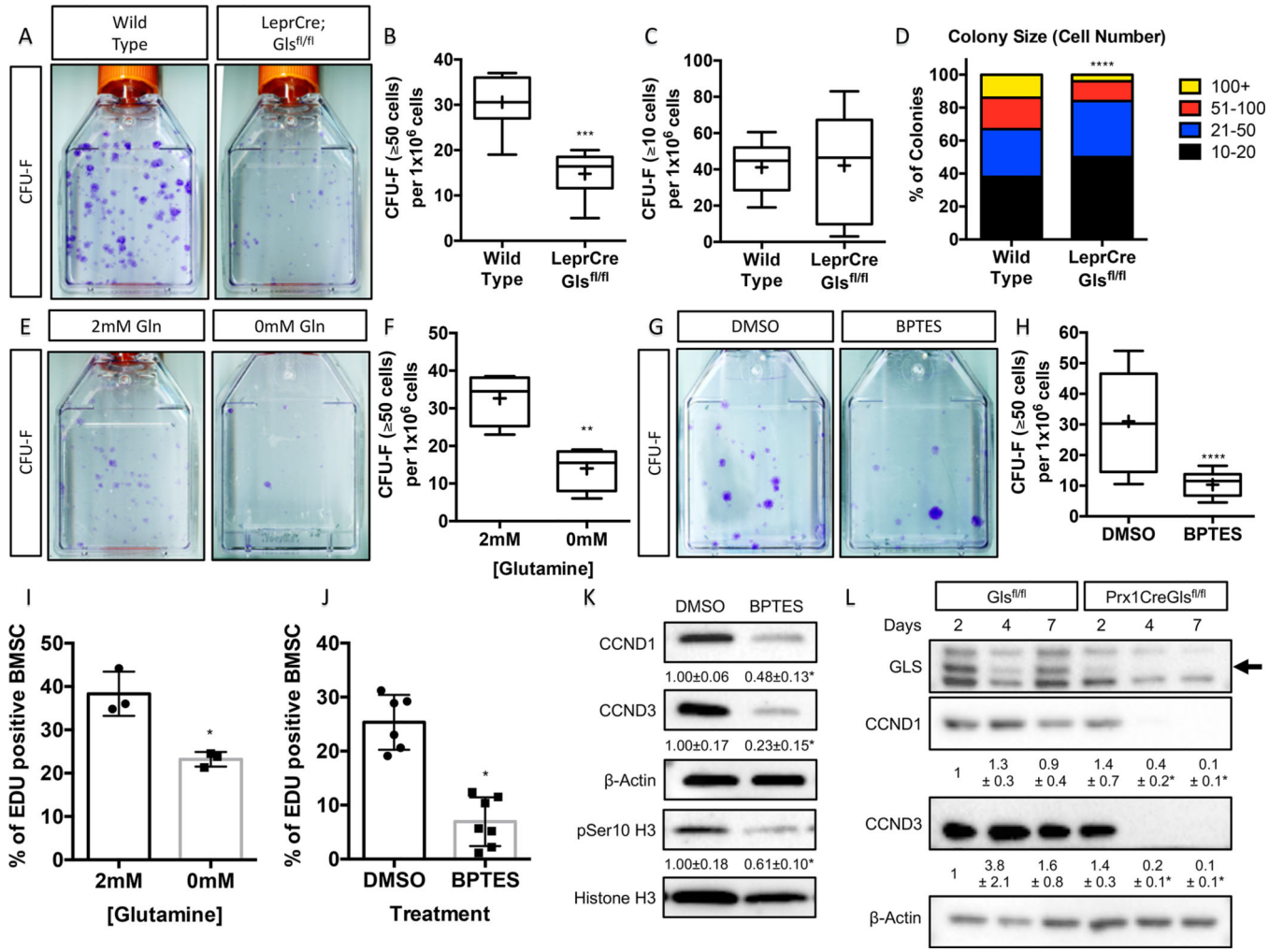

Figure 5: *Gls* activity is required for SSC proliferation and expansion.

(A) Colony forming unit (CFU) assay of 4-month old *LeprCre;Gls*$^{fl/+}$ (Wild Type) or *LeprCre;Gls*$^{fl/fl}$ mutant littermates. **(B-C)** Tukey box and whisker plots of the number of colonies per mouse containing greater than 50 cells **(B)** or greater than 10 cells **(C)**. **(D)** Prevalence of colonies binned for cell number. N ≥ 208 colonies from 6 animals. **(E-H)** CFU assay **(E,G)** or Tukey box and whisker plots **(F,H)** showing the effect of glutamine withdrawal **(E-F)** or GLS inhibition treatment **(G-H)** on the number of colonies containing at least 50 cells isolated from 4-month old *C57Bl/6* wild type mice. n=6 mice. **(I-J)** Effect of glutamine withdrawal **(I)** or **(J)** GLS inhibition on EDU incorporation in SSC. **(K)** Western blot analyses of the effect of GLS inhibition on cell cycle protein expression in ST2 cells. **(L)** Western blot analyses of cell cycle markers in SSC cultured in mineralization media for up to 7 days. Phosphorylated-Histone H3 normalized to total Histone H3; others normalized to β-Actin. Fold change ± SD relative to control for 3 independent experiments. *p≤0.05, **p≤0.005, ***p≤0.0005, ****p≤0.00005. See also Figure S6.

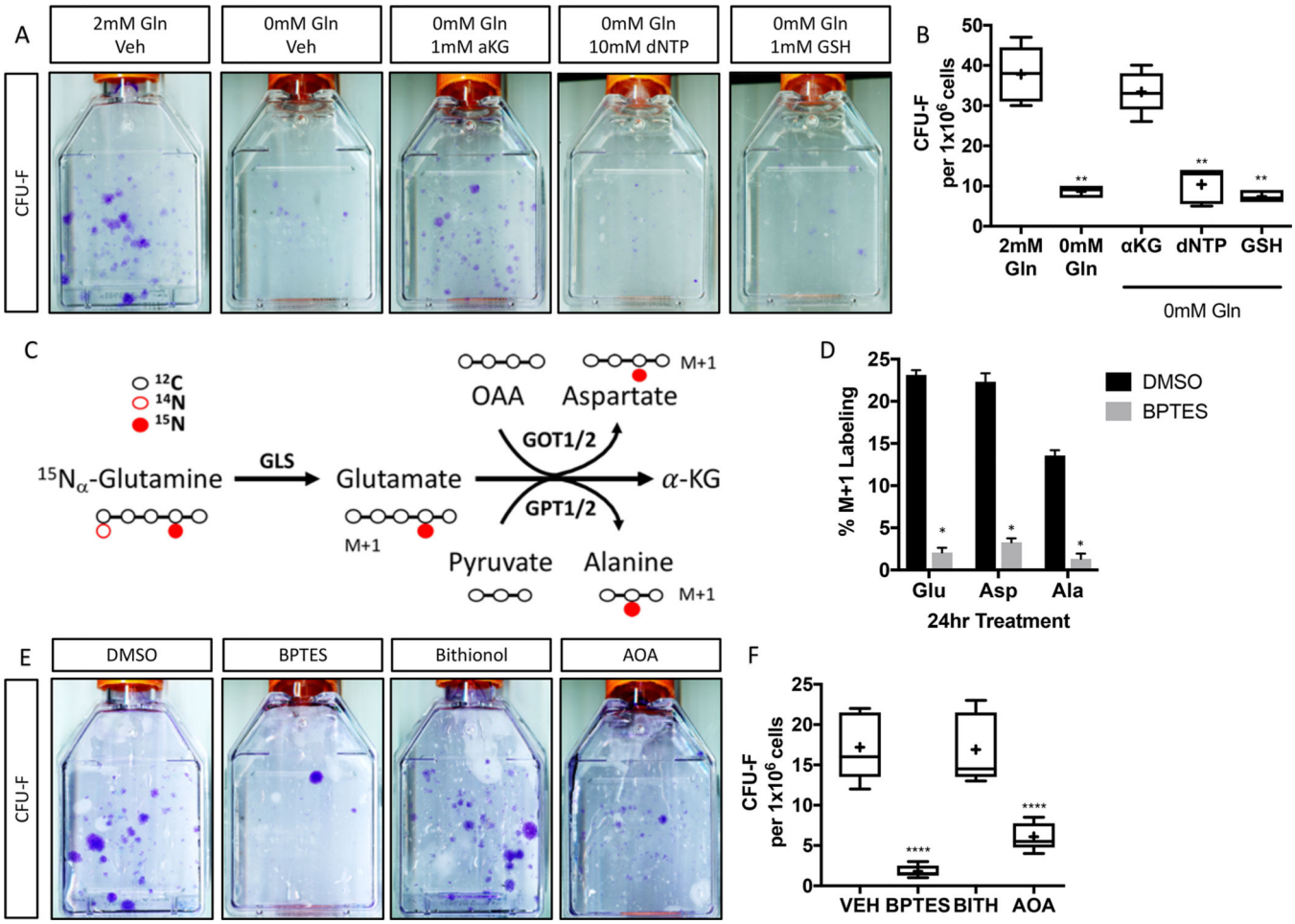

Figure 6: Transaminase dependent αKG production is critical for SSC proliferation.

(A-B) CFU assay **(A)** or Tukey box and whisker plots **(B)** showing the effect of glutamine withdrawal and supplementation with downstream metabolites on colony formation in 4-month old *C57Bl/6* wild type mice. n=5 mice. **(C)** Graphical depiction of tracing glutamine metabolism using $^{15}N_{\alpha}$-glutamine. Red filled circles denote ^{15}N whereas black and red open circles denote ^{12}C and ^{14}N respectively. OAA – oxaloacetate. **(D)** The effect of BPTES treatment on the fractional contribution of $^{15}N_{\alpha}$-glutamine to glutamate, aspartate and alanine. **(E-F)**, CFU assay **(E)** or Tukey box and whisker plots **(F)** showing the effect of BPTES, AOA, or Bithionol on colony formation. n=5 mice.